

### 3D Cellular Automata Finite Element simulations of cleavage fracture initiation in the transition region

R. Cuamatzi-Melendez<sup>1,a</sup>, J. R. Yates<sup>2,b</sup>

<sup>1,2</sup> Mechanical Engineering Department, Sheffield University

Sir Frederick Mappin Building, Mappin Street, Sheffield, S1 3JD, UK

<sup>a</sup>ruben\_c\_m@yahoo.com.mx , <sup>b</sup>j.yates@sheffield.ac.uk

**Keywords:** Microcracks, cleavage, CAFE, micromechanisms.

**Abstract.** An existing hybrid modelling strategy based on a combination of cellular automata and finite element analysis (CAFE model) was extended to incorporate the distribution of different cleavage fracture nucleation sites found in a Grade A ship plate steel. The CAFE model combines the state variables of cellular automata within the framework of a finite element solver to dissociate microstructural properties from the solution of forces and displacements. In the present CAFE model four different cleavage fracture nucleating micromechanisms found from fractographic analyses were implemented. The model was able to simulate the Charpy fracture behaviour over the full range of the ductile-brittle transition.

#### Introduction

In the modelling of the ductile-brittle fracture transition in ferritic steels it is important to correctly identify the relevant fracture nucleation micromechanisms. It is well known that MnS inclusions are the important features controlling ductile fracture nucleation in structural steels. Cleavage fracture is usually regarded as being initiated by dislocation pile-ups or by grain boundary carbides. However, some evidence has been found for other micromechanisms of cleavage nucleation, both within grains and in grain boundaries [1-4]. These include the fracture of iron based carbides or carbides colonies; debonding of inclusions such as TiC and manganese sulphide; and the fracture of pearlite colonies.

The implementation of cleavage models in the simulation of the fracture of ferritic steels has usually been confined to a single micromechanism [5]. A more realistic approach would be to incorporate all the potential fracture mechanisms and allow free competition between them. Each micromechanism will have a different spatial distribution throughout the structure, a different temperature dependence and a different distribution of critical fracture stress, depending on the size of the initiating particles and the local grain size.

In this paper, we present work on identifying four cleavage micromechanisms in a Grade A ship plate steel and the incorporation of this information into a hybrid cellular automata finite element scheme to predict the Charpy fracture energy through the ductile-brittle transition temperature range.

#### Experimental work

The identification of cleavage nucleation micromechanisms was done using blunt four point double-notch bend specimens, as shown in figure 1. The specimens were tested at -196°C, -60°C, 0°C and 25°C in an Instron servo-hydraulic test frame. In these tests both notches were subjected to the same state of stresses and strains. When fracture initiates in one notch, the crack propagates from that notch but the surviving notch will have experienced the same critical state of stress and strain condition developed in the failed notch.

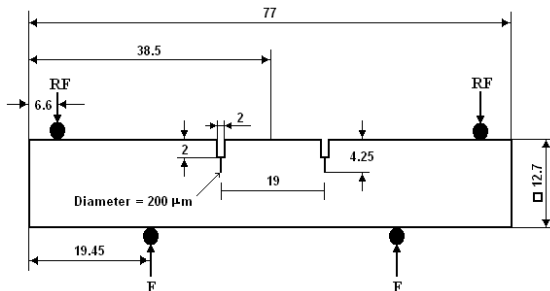


Fig. 1. Four point double-notch bend specimens.

The surviving notches were sectioned, polished and etched with mixture of 5% nital with a small amount of picral. Four micro micromechanisms were found at all test temperatures, as shown in figure 2. These are: debonding of inclusions in the ferrite grain boundaries; debonding of inclusions in the ferrite-pearlite boundary; fracture of the lamellar pearlite colonies; and cracked carbides in ferrite grain boundaries. The proportions of each micromechanism changed with temperature.

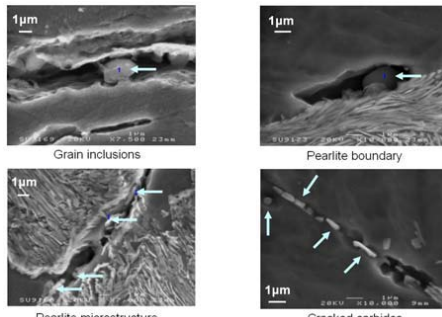


Fig. 2. Four cleavage fracture nucleation micromechanisms.

### The CAFE model

The implementation of the different micro features for cleavage nucleation was done with the CAFE model[5]. In this model, the Rousselier continuous damage model [6] was used to account for the ductile fracture process and the Beremin model [7] for the brittle part. Each set of cellular automata is linked to a different fracture mechanism and describes the whether a local region of the structure has failed or not. The size of each cell in each CA array defines the size scale appropriate to each failure mechanism. Therefore material failure information is moved from the finite elements and distributed across the CA arrays in a multiscale manner.

Two independent CA arrays with different size were created for ductile and brittle fracture. Cell sizes were chosen based on the key length scales of fracture mechanism: the distance between large microvoids for ductile fracture and cleavage facet size for brittle fracture. It was found that the appropriate brittle fracture scale corresponded to the size of the largest grains or to the size of groups of grains with small misorientation angle that behaved as a single facet.

A randomly generated critical value of the damage variable  $\beta_F$ , within a normal distribution taken from [5], is assigned to each ductile CA. A ductile cell dies when its damage variable exceeds the critical value. The load bearing capacity of that cell will be zero. This information is transferred to the finite element stiffness matrix, re-distributing the forces in the structure. After the ductile CA cells have been processed, the state of the ductile CA array,  $\Upsilon_{m(D)}$ , is mapped over the brittle CA

array,  $\Upsilon_{m(B)}$ . Since both CA arrays occupy the same physical space, any change in one array is reflected in the other array.

The brittle CA array was apportioned randomly according to the fractographic analysis so that 76% of the cells were ferrite grains and 24% were pearlite. Each microstructural phase has two of the four cleavage nucleation micromechanisms shown in figure 2. The fracture stress,  $\sigma_F$ , for each mechanism was calculated from equation 1 for carbide particle induced cleavage [8, 9] or equation 2 for fracture at grain boundaries [10]:

$$\sigma_F^{cf} = \sqrt{\frac{\pi E \gamma_{ef}}{(1-\nu^2)d_c}} \quad (1)$$

where  $\sigma_F^{cf}$  is the fracture stress of a carbide-ferrite interface,  $\gamma_{ef}$  is the effective surface energy of a carbide-ferrite interface,  $d_c$  is the carbide size,  $E$  is the modulus of elasticity and  $\nu$  is the Poisson's ratio.

$$\sigma_F^{ff} = \sqrt{\frac{\pi E \gamma_{ff}}{(1-\nu^2)d_g}} \quad (2)$$

Furthermore,  $\sigma_F^{ff}$  is the fracture stress of a ferrite-ferrite interface,  $\gamma_{ff}$  is the effective surface energy of a ferrite-ferrite interface, and  $d_g$  is the ferrite grain size.

The size of the initiating carbides was determined from fractographic analysis and the Weibull distribution shape and scale parameters were determined for  $d_c$  in equation (1). Similarly, grain sizes and grain orientation angles were determined and the shape and scale parameters of the Weibull distributions were used to create random values of  $d_g$  and  $\theta$  in equation (2). Hence, all the cells in the brittle CA array have different fracture strengths depending on the micromechanism attributed to the cells.

A finite element solver is used to determine the maximum principal stress in the brittle CA cells. Fracture will propagate from a dead brittle cell  $m$  to a neighbouring cell  $l$  if the maximum principal stress at cell  $l$  exceeds its fracture stress and the misorientation angle between these two cells,  $|\theta_m - \theta_l|$  is smaller than the misorientation threshold,  $\theta_F$ . The finite element stiffness matrix is modified by a change in the state of either the ductile or brittle cells, and this creates local strain concentrations in the regions of crack nucleation and growth.

### Simulation of cleavage nucleation sites

The validity of the new approach was tested by modelling the fracture of the four point double-notch bend specimens over a range of temperatures and examining the distribution of cleavage initiation sites. These were compared with the distribution of sites found from the fractographic examination. Figure 4 shows the Abaqus® 3D finite element model and a close-up view of the notch root where the CAFE model was applied.

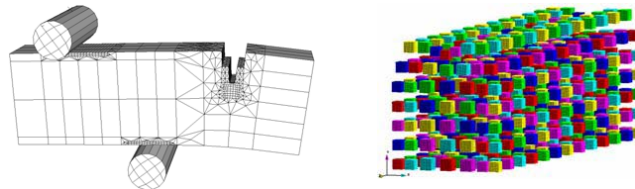


Fig. 4. Finite element model of four point double-notch bend tests and the array of cells in the notch root.

The damage zone consisted of 637 C3D8R 8-node finite elements. The size of the finite elements of the damage zone was around  $0.5\text{mm}^3$ .  $5 \times 5 \times 5$  ductile and  $10 \times 10 \times 10$  brittle CA arrays were created in each finite element in the damage zone. The ductile damage cell size is  $L_D \approx 0.5/5 = 0.1\text{mm}$  and the brittle damage cell size is  $L_B \approx 0.5/10 = 0.05\text{mm}$ . The model will therefore have 79625 ductile and 637000 brittle CA cells. Due to symmetry, only a quarter of the specimen was modelled.

The distributions of microcracks from the CAFE model and the experiments are shown in figure 5 for all test temperatures. Most of cleavage initiation points nucleated within 1mm of the notch root. The results showed that the distribution of cleavage fracture initiation points agrees well with those found experimentally.

Calibration of the ductile damage model was done by comparison of CAFE models with plain and notched tensile tests following Batisse *et al.* [11] and also by comparison with upper shelf Charpy data. For this a 3D finite element model of the Charpy test was created, as shown in figure 6. The damage zone consisted of 2100 C3D8R 8-node reduced integration finite elements. All the finite elements in the damage zone were about  $0.5\text{mm}^3$ , 125 and 1000 ductile and brittle cells were created in each FE. The CAFE model has 262500 ductile and 2100000 brittle CA cells.

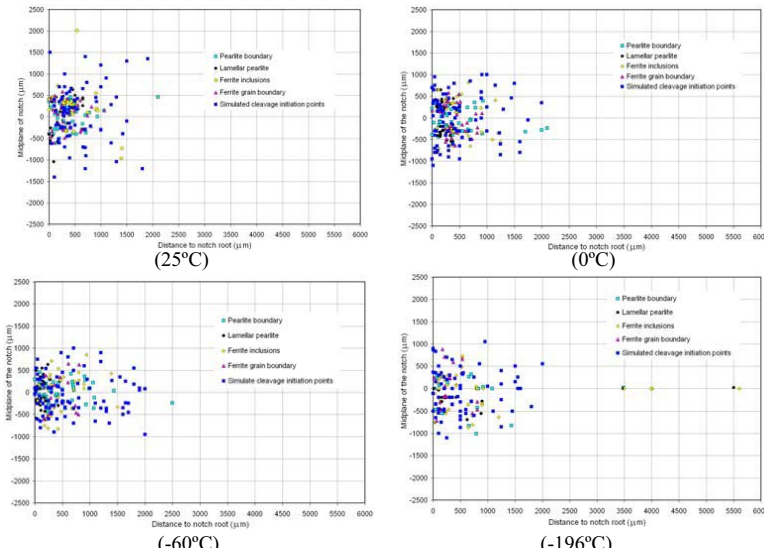


Fig. 5. Experimental and CAFE correlation of initiation points at  $-60^\circ\text{C}$ .

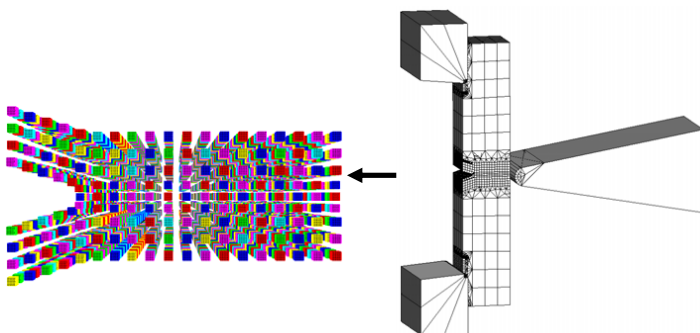


Fig. 6. Charpy test and the CA arrays created in the damage region.

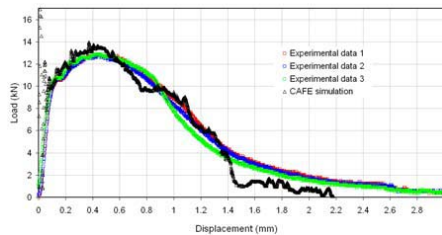


Fig. 7. Numerical against experimental correlation of a Charpy tests.

Figure 7 shows good correlation between numerical against experimental data in the upper shelf after fitting the ductile damage parameters.

The new cleavage modelling strategy was tested by simulating the Charpy fracture energy through the ductile-brittle transition of the ship plate steel, as shown in Figure 8.

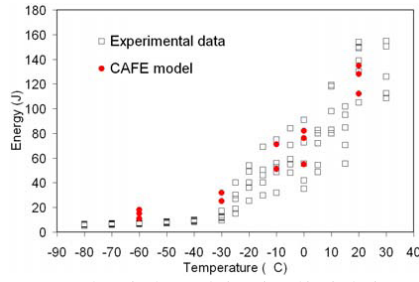


Fig. 8. CAFE simulation of the ductile-brittle transition.

## Discussion

The new cleavage modelling approach was able to simulate both the rise in Charpy impact energy with increasing temperature and the typical scatter in the transition region. This arises from introducing the distribution of the physically based parameters using random number generators in both CA arrays. In each simulation run, the CAFE model assigns different values of the damage model parameters, resulting in scatter in a unique Charpy energy value.

At -60°C, with 100% cleavage fracture, the simulated results were higher than the experimental values. This difference may be caused by the fact that fracture cannot cross the finite element boundary due to the limitations of the Abaqus® code.

## Conclusions

The multiscale nature of the CAFE model, and its intrinsic feature of separating the modelling of the fracture events from the calculation of the deformation of the structure, makes it ideally suited to the task of simulating failure arising from a range of competing mechanisms.

## References

- [1] Zhang, X. and J. Knott, The statistical modelling of brittle fracture in homogeneous and heterogeneous steel microstructures. *Acta Mater.*, 2000. **48**: p. 2135-2146.
- [2] Gibson, G., M. Capel, and S. Druce, Effect of heat treatment on the fracture toughness transition properties of an A508 Class 3 steel. In: Blauel J, Schwalbe K - H, editors. *Defect assessment in components - fundamentals and applications*, ESIS/EGF9. Mechanical Engineering Publications., 1991: p. 587-611.
- [3] Rosenfield, A. and D. Shetty, Cleavage fracture of steel in the upper ductile-brittle transition region. *Engng Fract Mech*, 1973. **17(5)**: p. 461-470.
- [4] Liu, Z., Cleavage fracture initiated by pearlite packets. *Iron Steel*, 1982. **17**: p. 12.
- [5] Shterenlikht, A. and I.C. Howard, The CAFE model of fracture - application to a TMCR steel. *Fatigue Fract Engng Mater Struct*, 2006. **29**: p. 770-787.
- [6] Rousselier, G., Ductile fracture models and their potential in local approach of fracture. *Nuclear Engineering and Design*, 1987. **105**: p. 97-111.
- [7] Beremin, F.M., A local criterion for cleavage fracture of a nuclear pressure vessel steel. *Metallurgical Transactions*, 1983. **14A**: p. 2277-2287.
- [8] Smith, E., The formation of a cleavage crack in a crystalline solid - I. *Acta Metallurgica*, 1966a. **14**: p. 985-989.
- [9] Smith, E., The formation of a cleavage crack in a crystalline solid - II. *Acta Metallurgica*, 1966b. **14**: p. 991-996.
- [10] Lin, T., A.G. Evans, and R.O. Ritchie, Stochastic modeling of the independent roles of particle size and grain size in transgranular cleavage fracture. *Metallurgical and Materials Transactions A*, 1987. **18A**: p. 641-651.
- [11] Batisse, R., et al., Ductile fracture of a 508 Cl 3 steel in relation with inclusion content: The benefit of the local approach of fracture and continuum damage mechanics. *Nuclear Engineering and Design*, 1987. **105**: p. 113-120.